The following publication X. Lyu, Y. Jia and Z. Xu, "A Novel Control Strategy for Wind Farm Active Power Regulation Considering Wake Interaction," in IEEE Transactions on Sustainable Energy, vol. 11, no. 2, pp. 618-628, April 2020 is available at https://doi.org/10.1109/TSTE.2019.2899087.

A Novel Control Strategy for Wind Farm Active Power Regulation Considering Wake Interaction

Xue Lyu, *Student Member, IEEE,* Youwei Jia, *Member, IEEE,* Zhao Xu, *Senior Member, IEEE*

***Abstract*—Given the ever-increased penetration of wind power generation in today's power systems, wind farms tend to operate in a dispatchable way to a certain extent by actively fulfilling dispatch orders from system operators. This paper is focused on the challenging issue of coordinating the interactive wind turbines in a wind farm, which are influenced by non-negligible wake effect, to efficiently respond to external dispatch order. To achieve this, a novel control strategy is proposed by 1) effectively allocating power regulation task to individual wind turbines; and 2) utilizing the existing resources (i.e. rotational kinetic energy and pitching capability) of wind turbine to satisfy the dispatch order efficiently and reliably. Extensive case studies on both constant and variable wind speed conditions are carried out to demonstrate the effectiveness of the proposed control strategy. As a comparison, simulations results based on uniform load sharing strategy are also presented. It is exhibited that our proposed strategy has better control performance in terms of total energy harvesting and pitching activation frequency.**

***Index Terms*—wind farm, wake effect, active power regulation, rotational kinetic energy, pitching capability**

NOMENCLATURE

P_{wt}	Mechanical power captured by WT
R	Rotor blade radius
C_{p}	Power coefficient
λ	Tip speed ratio
β	Pitch angle
ω_r	Rotor speed
v	Wind speed
P_{wt}^{mpp}	Mechanical captured by WT under MPPT mode
δv	Velocity deficit
C_{T}	Thrust coefficient
A	Area swept by rotor blades
A^{shadow}	Area of wind turbine under shadowing
D	Diameter of rotor blade
J	Equivalent inertia of wind turbine
H	Inertia constant
P_{KE}	Charging/discharging power in the form of rotor speed accelerating
$\omega_{r\max}$	Maximum rotor speed
$\omega_{r\min}$	Minimum rotor speed
ω_{rmpp}	Rotor speed under MPPT mode
P_{KE}^{cha}	Charging power in the form of rotor deceleration
P_{KE}^{disc}	Discharging power in the form of rotor deceleration
$P_{e\min}^{rot}$	The minimum output power of wind turbine with KE fully charged
$P_{e\max}^{rot}$	The maximum output power of wind turbine with KE fully discharged
ΔP_{rot}^{de}	Available charging range of KE
ΔP_{rot}^{ov}	Available discharging range of KE
ΔP_{wt}	Active power regulation task of individual WT
P_{wt}^{act}	Measured actual power output of WT
P_{WF}^{com}	Dispatch command of the WF
P_{WF}^{act}	Measured actual power output of WF

I. INTRODUCTION

THE increasing penetration of electronic converter interfaced renewable energy casts severe challenges on power system stability and reliability [1]. Wind generation has become one of the most promising renewable resources due to its relatively mature technology and thus widely deployed. However, the stochastic nature of wind energy makes it non-dispatchable in the power systems based on conventional control schemes. Typically, the traditional power plants should serve as backup resources to undertake wind power uncertainties, which turns out to be less economical and limit further development of wind energy. Therefore, it is expected that wind farm (WF) generation should meet the certain requirements given by system operators [2, 3].

To manage wind power uncertainties, one kind of feasible solutions is to install energy storage system (ESS) [4-7], including but not limited to pumped storage, flying wheel or super-capacitors. However, this kind of solutions has to involve excessive investment and complex control algorithms for ESS. Alternatively, another possible solution is to effectively utilize the existing resources of the WF to participate in active power ancillary service support.

Generally, control strategies that utilize the existing resources to achieve the controllability of wind power output could be classified into two categories, i.e., rotor speed regulation based control [8-11] and pitch angle regulation based control [12-14]. The rotor speed control exploits the kinetic

This work was supported by Hong Kong RGC Theme Based Research Scheme Grants No. T23-407/13N and T23-701/14N.

X. Lyu is with the Department of Electrical and Electronic Engineering, Southern University of Science and Technology, Shenzhen, China, and also with the Department of Electrical Engineering, The Hong Kong Polytechnic University, Hung Hom, Hong Kong. (email: xue.lyu@connect.polyu.hk)

Y. Jia is with the Department of Electrical and Electronic Engineering, Southern University of Science and Technology, Shenzhen, China, jiayw@sustc.edu.cn)

Z. Xu is with the Department of Electrical Engineering, The Hong Kong Polytechnic University, Hung Hom, Hong Kong. (email: eezhaoxu@polyu.edu.hk).

energy (KE) stored in the rotating mass to extend wind power output. Specifically, WTs can withhold power output and store partial energy in its rotating mass via rotor speed acceleration in an over-generation situation. On the other hand, the stored KE can be released back to the system through rotor speed deceleration in over-consumption situations while wind power output can incur a dip to replenish the KE during the rotor speed recovery period [15]. Even though the operating point of WT is shifted away from maximum power point (MPP) when such control is adopted, it has merit on energy harvesting since a certain amount of the curtailed energy is stored in the form of KE. The captured wind energy can also be regulated via adjusting the blade pitch angle. However, without deloading in advance, pitch angle control is only applicable to over-generation situation as it does not possess energy storage capability. In addition, it is worth noting that pitch angle is less desirable as its frequent activation leads to irreversible mechanical stress and fatigue.

The WF can become dispatchable source and follow the generation signal requested by system operator given a proper strategy. In [16], the supply-demand balance is achieved by controlling the utilization level of each WT to a common value. A two-layer structured active power regulation scheme is proposed in [17, 18], in which the upper layer controller coordinate the operating status of all WTs, and the lower layer controller regulate the power output of WT. In [17], the power reference sent to each WT is generated via the distributed model predictive control. To minimize wind energy loss, [18] allocates the power signal references among multiple WTs via a centralized optimal dispatch strategy. However, turning to a whole WF level, the naturally existing wake effect (i.e. As wind flow proceeds downstream, there exists a trail where wind speed is reduced) shall not be neglected. Due to the aerodynamic coupling, WTs in a WF exposes to different wind speeds and operates in different status. As a result, their active power regulation capabilities through rotor speed control and pitch angle control are different. By far, research work on WF active power regulation considering detailed wake model is still at its early stage [19,20] due to the complexity involved in the wake model. Considering the energy compromised by each WT in a WF is not equal, [19] proposes a variable utilization level control scheme for the WF, in which the utilization level of each WT is linear-inversely proportional to its rotor speed. In [20], the KE storage potential of the WTs is utilized to provide a buffer for power dispatch, and a consensus-based algorithm is adopted to obtain the same KE utilization ratio among all WTs. Though optimization methods can coordinate WTs and enable them to optimally work at the desired operating state, the solutions can be time-consuming to find given the high complexities involved in wake models, especially the scale of the WF is large. In addition, the wind speed and load demand are perpetually varying, which gives rise to an online application problem.

To overcome the existing limitations, we further investigate the cooperation among WTs to maintain the dispatch order in presence of wake effect from control point of view. In this paper, an adaptive method to allocate the active power regulation task to individual WTs is proposed at the supervisory WF control level, which achieves the objective of adequately exploiting the variable rotor speed range as the energy buffer and mitigating the frequent action of blade pitch angle. Specifically, the adjustable margin of WTs active power output through rotor speed control is determined via the estimation of the maximum absorbable/extricable energy from its rotational mass. It is worth noting that the proposed adaptive strategy is advantageous over other control methods without considering the cooperation among multiple WTs in terms of: 1) wind turbine system-friendliness (i.e. less actuation time of pitching control to reduce operational wear outs); 2) energy utilization efficiency; 3) over-/under-production capability of wind turbines at instant moments; and 4) control efficiency. Detailed comparisons are presented in Section V. The type-3 WT model is adopted to develop a detailed WF model, and the system model is built in DIgSILENT/PowerFactory. The effectiveness of the proposed control strategy is verified under different scenarios, where wind speed fluctuation and load variation are both considered. Simulation results exhibit promising control performance of the proposed strategy in terms of total energy harvesting and pitching activation frequency.

The next of the paper is organized as follows. The wind turbine modelling and wake effect modelling are described in Section II. Active power regulation methods of the wind turbine are presented in Section III. The proposed adaptive power dispatch strategy for the wind farm is presented in Section IV. Simulation studies and the paper are discussed and concluded in Section V and VI respectively.

II. Wind Turbine and Wake Effect Models

A. DFIG Model

Doubly fed induction generator (DFIG) is a popular wind turbine system owing to its relatively low rated power of the embedded converter. DFIG-based wind turbine system consists of wind turbine, gear-box, induction generator and a back-to-back converter, which is shown in Fig. 1. ω_r is rotor speed; i_r is rotor current; i_g is grid current; V_{dc} is DC-link voltage; β_{ref} is pitch angle reference; P_{ref} is active power reference obtained by the MPPT curve. The stator is directly connected to grid, and the rotor is interfaced with the grid through a back-to-back converter, of which the power capacity is about 20-30 percent of WT nominal capacity. The back-to-back converter is dedicated for generating electricity power, where the instantaneous current with varying amplitudes and frequency are synchronized to the main grid. The MPPT control is achieved by the rotor side converter (RSC) and the DC-link voltage is regulated by the grid side inverter (GSC).

The mechanical power extracted from the wind is defined as,

$$P_{wt} = \frac{\rho}{2}\pi R^2 v^3 C_p(\lambda,\beta) \tag{1}$$

where ρ is air density, R is rotor blade radius, v is wind speed, λ is the tip speed ratio, β is pitch angle, and C_p is power coefficient. Power coefficient represents a nonlinear relationship between the tip speed ratio and pitch angle. As

formulated in [21], it can be expressed as,

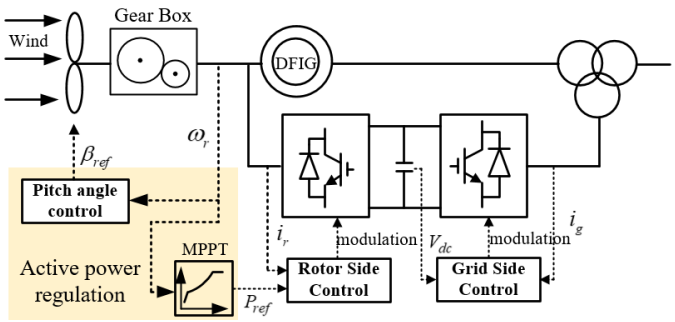

Fig.1 DFIG wind turbine configuration

$$C_p = 0.22(\frac{116}{\lambda_i} - 0.4\beta - 5)e^{-\frac{12.5}{\lambda_i}} \tag{2}$$

$$\frac{1}{\lambda_i} = \frac{1}{\lambda + 0.08\beta} - \frac{0.035}{\beta^3 + 1} \tag{3}$$

where the tip speed ratio is defined as,

$$\lambda = \frac{\omega_r R}{v} \tag{4}$$

Normally, the pitch angle equals to zero in case that v is lower than the rated value. That is, C_p is only correlated with λ. According to Eq. (4), there exists an optimal rotor speed value that yields maximal power coefficient $C_{p\max}$ for a given wind speed, and the captured power by WT can be expressed as,

$$P_{wt}^{mpp} = \frac{\rho}{2}\pi R^2 C_{p\max} v^3 \tag{5}$$

B. Wake Effect Model

Wind turbines extract energy form wind and there exists a wake behind the turbine. Generally, the layout of the WF and the operation status of each WT would determine the wake effect. The power production of the WF is affected by the aggregated influence of wake effect. Recently, several wake models have been proposed. Jensen's wake model is one of the most prevalent one and is suitable for engineering applications [22]. In this work, the Jensen's model is adopted to describe the wake effect. It is established based on the assumption that the wake expands linearly downstream, as shown in Fig. 2. The velocity profile of the wake generated by turbine i (assuming there are totally N wind turbines in wind farm) can be given by,

$$v_i = v_0(1 - \delta v_i) \tag{6}$$

where v_0 is the free wind speed, δv_i is the aggregated velocity deficit. It is noted that the effective wind speed of wind turbine i is not only affected by the upstream wind turbine that is directly in front of it, but also other upstream wind turbines. In considering multiple wakes formed by multiple upstream wind turbines, the aggregated velocity deficit of wind turbine i can be calculated as,

$$\delta V_i = \sqrt{\sum_{j\in N: x_j<x_i} (\delta V_{ij})^2} = \sqrt{\sum_{j\in N: x_j<x_i} ((1-\sqrt{1-C_{Tj}})(\frac{D_j}{D_j + 2k(x_i - x_j)})^2 (\frac{A_{j\to i}^{shadow}}{A_i}))^2} \tag{7}$$

where D_j is the diameter of the turbine j blades; C_{Tj} is the thrust coefficient of the turbine j, which also represents a nonlinear relationship between the tip speed ratio and the pitch angle. The thrust coefficient can be obtained through a look-up table or curve fitting [23, 24], as given in Fig. 3. $x_i - x_j$ is the distance of upstream turbine j and downstream turbine i along with the wind direction. k is the roughness coefficient, it has a default value of 0.075 for farmlands and 0.04 for offshore locations. $A_{j\to i}^{shadow}$ is the overlap between the area spanned by the wake shadow cone generated by turbine j and the area swept by the turbine i (A_i). $A_{j\to i}^{shadow}$ can be calculated using the following relationship,

$$A_{j\to i}^{shadow} = (D_i + 2k(x_i - x_j))^2 \cos^{-1}(\frac{L_{ij}}{D_i + 2k(x_i - x_j)}) + D_i^2 \cos^{-1}(\frac{d_{ij} - L_{ij}}{D_i + 2k(x_i - x_j)}) - d_{ij} z_{ij} \tag{8}$$

where d_{ij} is the distance between the centre of downstream wind turbine and the centre of the wake effect, L_{ij} is the distance between the centre of the wake effect and the shadow area.

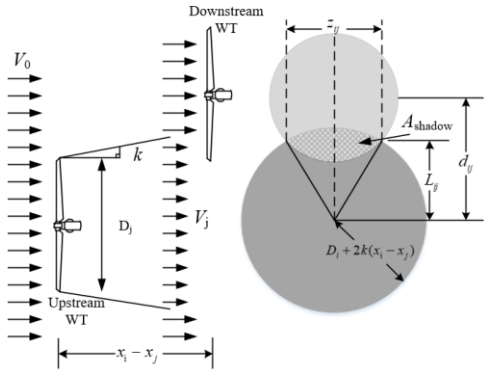

Fig.2 Jensen's wake model

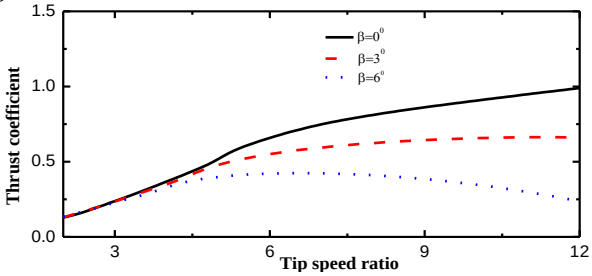

Fig.3 Thrust coefficient

III. Active Power Control Measures of Wind Turbine

In this section, principles of utilizing rotor speed regulation based control and pitch angle regulation based control to adjust wind power output are discussed respectively. In addition, the energy loss brought along by different control measures in deloading situation is analyzed.

A. Rotor Speed Regulation based Control

The essential idea of rotor speed control is to utilize the KE stored in the rotating rotor to expand active power output (i.e. $\pm\Delta P$). The corresponding dynamic process is explained in Fig. 4. It is assumed that the WT initially operates at point A under MPPT control. Once the power regulation task is received, the MPPT mode is bypassed and the power deviation is added to the initial power reference. Due to the fast response of power electronic devices, the electrical power output can be modified rapidly. However, the turbine mechanical power is remaining

near the initial point. The mismatch between the electrical and mechanical power forces rotor speed acceleration/deceleration and the stored/released KE can be utilized as an energy buffer. For example, if less wind power production is expected, the operating point will be shifted to point B by charging KE for power deduction. On the contrary, if the dispatch command is greater than MPP, WT will be controlled to shift to point D by releasing KE and maintained stable eventually via returning to point A.

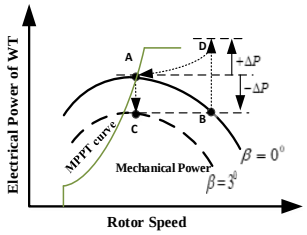

Fig. 4. Control dynamics for rotor speed control and pitch angle control

B. Pitch Angle Regulation based Control

Under WTs' MPPT control, pitch angle control is activated to limit the rotor speed at the predefined threshold. To offer active power regulation service, pitch angle control has to activate more frequently than before. The dynamic process of pitching control to adjust wind power output (i.e. $-\Delta P$) is illustrated in Fig. 4. Basically, when the introduced power command is less than the actual power output, WT shifts to point C by increasing pitch angle. Distinguished from rotor speed control, pitching control does not possess energy storage capability and thus cannot provide overloading support.

C. Wind Energy Loss Analysis

For a single WT, if the deloading coefficient is determined, the captured wind power can be expressed as,

$$P_{wt}^{del} = \frac{1}{2}\rho A C_{pdel}(\lambda,\beta)v^3 \tag{9}$$

where C_{pdel} is defined as the deloading power coefficient.

According to above-mentioned analysis, the captured wind power can be regulated via rotor speed control or pitch angle control. Since their control mechanisms are different, the corresponding wind energy loss in deloading situation is also different and will be illustrated respectively in the following.

1) *Rotor Speed Control:*

For a WT, the KE stored in its rotating mass can be expressed as,

$$E = \frac{1}{2}J\omega_r^2 \tag{10}$$

where J denotes the equivalent inertia of the WT.

Rotor speed variation is a result of the imbalance between the captured wind power and electric power. The charging/discharging power in the form of KE variation can be calculated via the differential of Eq. (10). In MPPT control mode, the electric power reference is generated via the MPPT curve. To ensure that the wind turbine can be a dispatchable source, it should no longer operate at the MPPT control mode. Instead, the dispatch command is sent to the wind turbine and is tracked as the new active power reference. This dynamic process can be expressed as,

$$P_{wt} - P_e = P_{wt} - P_{com} = \frac{dE}{dt} = J\omega_r\frac{d\omega_r}{dt} = P_{KE} \tag{11}$$

where P_{com} is the dispatch command and P_{KE} is the charging/discharging power.

The inertia constant of the WT is generally defined as,

$$H = \frac{J\omega_{rbase}^2}{2P_{wtN}} \tag{12}$$

where P_{wtN} is the rated power of WT, ω_{rbase} is the base value of the angular speed.

Based on the definition of H, Eq. (11) can be rewritten as Eq. (13) in per-unit form,

$$P_{wt[pu]} - P_{com[pu]} = 2H\omega_{r[pu]}\frac{d\omega_{r[pu]}}{dt} \tag{13}$$

By integrating Eq. (13) over time t_0 to t_1, in deloading situation, the total energy production of the WF under rotor speed regulation based control is obtained,

$$\begin{aligned} E_{wt}^{rot} &= \int_{t_0}^{t_1}\sum_{i=1}^{N}P_{wti}dt = \int_{t_0}^{t_1}P_{WF}^{com}dt + 2H\int_{t_0}^{t_1}\sum_{i=1}^{N}\omega_{ri}d\omega_{ri} \\ &= \int_{t_0}^{t_1}P_{WF}^{com}dt + H\sum_{i=1}^{N}(\omega_{ri1}^2 - \omega_{ri0}^2) \end{aligned} \tag{14}$$

where N is the number of WTs in the WF.

In contrast, the total wind energy production of the WF under MPPT control can be described as,

$$E_0 = \int_{t_0}^{t_1}\sum_{i=1}^{N}P_{wti}^{mpp}dt \tag{15}$$

According to Eq. (14) and (15), the wind energy loss when rotor speed regulation based control is adopted can be expressed as,

$$E_{loss}^{rot} = E_0 - E_{wt}^{rot} = \int_{t_0}^{t_1}(\sum_{i=1}^{N}P_{wti}^{mpp} - P_{WF}^{com})dt - H\sum_{i=1}^{N}(\omega_{ri1}^2 - \omega_{ri0}^2) \tag{16}$$

It can be found that the sacrificed wind energy caused by providing active power regulation service is reduced, as partial curtailed power is stored in the rotational rotor in the form of KE via rotor speed acceleration.

2) *Pitch Angle Control:*

Different from rotor speed control, when pitch angle control is activated to curtail wind power capture, the power coefficient is directly decreased without rotor speed acceleration. Accordingly, the total wind energy production under pitching based deloading control can be expressed as,

$$E_{wt}^{pit} = \int_{t_0}^{t_1}\sum_{i=1}^{N}P_{wti}dt = \frac{1}{2}\int_{t_0}^{t_1}P_{WF}^{com}dt \tag{17}$$

According to Eq. (15) and (17), the wind energy loss brought along by pitching based deloading control can be expressed as,

$$E_{loss}^{pit} = E_0 - E_{wt}^{pit} = \int_{t_0}^{t_1}(\sum_{i=1}^{N}P_{wti}^{mpp} - P_{WF}^{com})dt \tag{18}$$

Compared with Eq. (16), it can be found that the main difference of energy loss between rotor speed regulation and pitch angle regulation lies in the KE alternation. Apart from the advantage on energy harvesting, there are other two reasons that why rotor speed control should be prioritized. The first one lies

in its fast response since rotor speed can be controlled through electronic converters. The second one is that the frequent activation of blade pitch angle inevitably leads to irreversible fatigue of WT.

IV. Proposed Adaptive Power Dispatch Strategy in Wind Farm

To adequately exploit the KE storage capability as an energy buffer and mitigate the frequent action of pitch actuator while follow the dispatch order, the cooperation between WTs in the WF should be investigated. Taken wake effect into consideration, this section proposes an adaptive method to allocate the active power regulation task to individual WTs.

A. Active Power Dispatch in Deloading Situation

When the required generation is less than WF power production, a deloading control should be implemented. To track the dispatch command, a possible approach is to equally distribute the deloading requirement to each WT. However, when the wake interaction is considered, this is no longer an optimal solution. It is easy to understand that the charging range of downstream WTs' KE is larger than upstream WTs' due to the wake effect. The same deloading requirement will bring about the consequence that the pitch angle control of upstream WTs activates frequently while the KE of downstream WTs is always not fully charged. To adequately exploit the energy buffer and reduce activation frequency of pitch angle control, the deloading task should be allocated adaptively according to the KE charging range of each WT. It should be noted that the implementation of rotor speed control generates impact on energy harvesting capability of down WTs due to wake interactions. As shown in Fig. 3, the thrust coefficient increases along with rotor speed acceleration, which leads to the decrease of wind speed reaching downstream WTs, and in turn their output power. To enhance total energy harvesting, the response priority of rotor speed control for different row WTs should be considered when assigning deloading task. According to the wake characteristic, the KE charging priority of different rows WTs is predefined as per from back row to front row in sequence. In the situation that KE of all WTs is fully charged yet the required deloading is still not achieved, the pitch angle control has to activate. Similarly, the implementation of pitch angle control affects the operation status of down WTs. It can be seen from Fig. 3 that the increase of pitch angle leads to thrust coefficient reduction, and then wind speed reaching downstream WTs increases. Accordingly, to reduce mechanical fatigue, the response priority of pitch angle control is also defined from back row to front row in sequence.

Once the activation priority of the deloading control for each row WTs is determined, the deloading task among all WTs should be allocated in accordance with their KE charging range. According to (11), the electrical power output of WT is determined by two terms. The first term is the captured wind power, and the second term is the energy stored/released by the rotational rotor. Specifically, the available KE charging range can be determined by its current rotor speed and the maximum rotor speed, which can be formulated as,

$$P_{\mathrm{KE}}^{cha} = \frac{\Delta E}{\Delta t} = P_{wtN} H \frac{\omega_{r\max}^2 - \omega_r^2}{\Delta t} \tag{19}$$

where Δt is the dispatch cycle.

Based on Eqs. (11) and (19), the WT output power with KE fully charged can be expressed as,

$$P_{e\min}^{rot} = \frac{1}{2}\rho A C_p(\omega_{r\max}) v^3 - P_{KE}^{cha} \tag{20}$$

The two different cases that deloading could be achieved via only utilizing rotor speed control or utilizing integration of rotor speed control and pitch angle control will be illustrated respectively in the following.

1) Deloading via Rotor Speed Control

Assuming there are *m* rows and each row consists of *n* WTs in the WF. When the required deloading can be achieved by only utilizing rotor speed control, as expressed in Eq. (21), the deloading task should be allocated adaptively according to the KE charging range of each WT to enhance total KE storage.

$$P_{WF}^{com} \geq m\sum_{i=1}^{n} P_{e\min i}^{rot} \tag{21}$$

The last row WTs has a high priority to assume the deloading task, which can be expressed as,

$$\Delta P_{wt,n} = \min\left\{\frac{m\cdot n}{m}\Delta P, \Delta P_{rot,n}^{de}\right\} = \min\left\{n\Delta P, \Delta P_{rot,n}^{de}\right\} \tag{22}$$

where ΔP is the power deviation between the actual output power of WF and the dispatch command (i.e. $\Delta P = P_{WF}^{act} - P_{WF}^{com}$), $\Delta P_{rot,n}^{de}$ is the deviation between the actual power output of the *n*-th row WT and $P_{e\min,n}^{rot}$. Eq. (22) ensures that if the deloading requirement is within the KE charging range of the last row WTs, the deloading task is allocated to each last row WT equally. Otherwise, the deloading task is allocated according to their available KE charging range. Based on the above-mentioned analysis, the deloading task allocated to the arbitrary upstream *i*-th row WTs can be expressed as,

$$\Delta P_{wt,i} = \min\left\{n\Delta P - m\sum_{j=i+1}^{n}\Delta P_{wt,j}, \Delta P_{rot}^{de,i}\right\} \tag{23}$$

It can be found that Eqs. (22) and (23) guarantee the deloading task is adaptively allocated to each WT according to their KE charging range and response priority, which is different from the uniform deloading allocation method.

2) Deloading via Integration of Rotor Speed Control and Pitch Angle Control

In the situation when the deloading requirement cannot be achieved by only utilizing rotor speed control, as expressed in Eq. (24), the pitch angle control has to be involved in.

$$P_{WF}^{com} < m\sum_{i=1}^{n} P_{e\min i}^{rot} \tag{24}$$

As mentioned above, for last row WTs, their pitching based deloading control has a high priority to response, and the deloading task can be calculated as,

$$\Delta P_{wt,n} = \min\left\{n\Delta P - m\sum_{i=1}^{n-1}\Delta P_{rot,i}^{de}, P_{wt,n}^{act}\right\} \tag{25}$$

where $P_{wt,n}^{act}$ is the actual output power of the *n*-th row WT. Eq

(25) ensures that only the excessive power production that cannot be transformed as KE is curtailed via pitch angle control. Similarly, for the *i*-th row WTs, the deloading task can be assigned according to,

$$\Delta P_{wt,i} = \min\left\{ n\Delta P - m(\sum_{j=1}^{i-1} \Delta P_{rot,j}^{de} + \sum_{j=i+1}^{n} \Delta P_{wt,j}), P_{wt,i}^{act} \right\} \quad (26)$$

where $P_{wt,i}^{act}$ is the actual output power of the *i*-th row WT. Eqs. (25) and (26) guarantee that the WTs' energy buffer is utilized adequately and the frequent action of pitch actuator is mitigated as much as possible while fulfilling the deloading requirement.

B. Active Power Dispatch in Overloading Situation

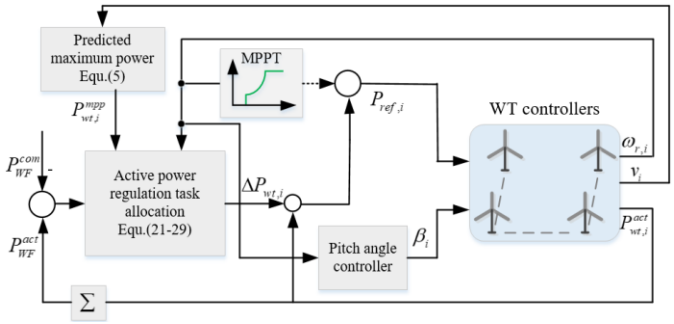

Fig. 5. The proposed adaptive active power regulation method for WF

When over-consumption appears event occurs, WF is expected to provide additional active power support, which is referred as overloading control. In this context, the stored KE should be released back to system. Similarly, when the wake interaction is considered, the cooperation among WTs should be investigated to ensure WTs stable operation and enhance total energy harvesting. As shown in Fig. 3, the thrust coefficient decreases along with rotor speed deceleration, which in turn increases wind power capture of down-WTs. Therefore, the overloading task allocation priority is defined from the front row WTs to the back row WTs in sequence.

It should be noted that the variable speed operation should be staying within the operating limits of the WT in overloading situation. The WT might stall if too much KE is extracted. According to [25], operating at a rotor speed that lower than the MPP one may reduce small signal stability. To avoid this problem, the maximum electrical power output of WT should be subjected to,

$$\begin{aligned} P_{e\max}^{rot} &= \frac{1}{2}\rho A C_p(\omega_{rmpp}) v_w^3 - P_{KE}^{disc} \\ &= \frac{1}{2}\rho A C_p(\omega_{rmpp}) v_w^3 - P_{wtN} H \frac{{\omega_{rmpp}}^2 - \omega_r^2}{\Delta t} \end{aligned} \quad (27)$$

where ω_{rmpp} is the rotor speed at MPP status, P_{KE}^{disc} is the discharging power through rotor speed deceleration.

The first row WTs has a high priority to shoulder the overloading task, which can be expressed as,

$$\Delta P_{wt,1} = \min\left\{ n\Delta P, \Delta P_{rot,1}^{ov} \right\} \quad (28)$$

where $\Delta P_{rot,1}^{ov}$ is the deviation between the actual output power of the *n*-th row WT and its $P_{e\max,1}^{rot}$. Eq. (28) ensures that the minimal value of WT overloading capability and the power deviation is selected. Otherwise, the excessive rotor speed deceleration may cause WTs trip off. If the power deviation still cannot be fully compensated via the fully discharging of the first front row WTs' KE, the remaining overloading task will be allocated to the neighbor downstream WTs. In this context, the overloading task of the *i*-th row WTs can be expressed as,

$$\Delta P_{wt,i} = \min\left\{ n\Delta P - m\sum_{j=1}^{i-1} \Delta P_{rot,j}^{ov}, \Delta P_{rot,i}^{ov} \right\} \quad (29)$$

Similarly, Eq. (28) guarantees the stable operation of the *i*-th row WTs.

To implement the proposed adaptive power dispatch control scheme, a wind farm central controller is established as shown in Fig. 5, where P_{WF}^{com}, P_{WF}^{act} are dispatch command and measured active power output of the WF, respectively; $\omega_{r,i}$, β_i, v_i, $P_{wt,i}^{act}$, $P_{wt,i}^{mpp}$, $P_{ref,i}$ are rotor speed, pitch angle, wind speed, measured active power, the maximum captured mechanical power and the active power reference of the *i*-th WT, respectively. The deloading/overloading task $\Delta P_{wt,i}$ can be readily and adaptively calculated and assigned to individual wind turbine according to Eqs. (21-29). During this dynamic active power regulation process, the wind speed reaching downstream WTs are influenced by wake interactions and can be calculated via wake equations (6) and (7). It should be noted the evaluation of KE charging/discharging range of each WT and the corresponding active power regulation task allocation can be realized rapidly, which ensures the applicability of proposed control strategy on online application.

V. Case Studies

To evaluate the performance of the proposed control strategy, a testing system comprising of two conventional synchronous generators (SGs), a DFIG-based WF with three rows and each row consisting of four WTs, and a fluctuated power load is constructed in DIgSILENT/PowerFactory, which is shown in Fig.6. The total capacity of the wind farm is 60-MW. The spacing of two adjacent DFIGs is 10R. Detailed simulation parameter settings are referred to Appendix.

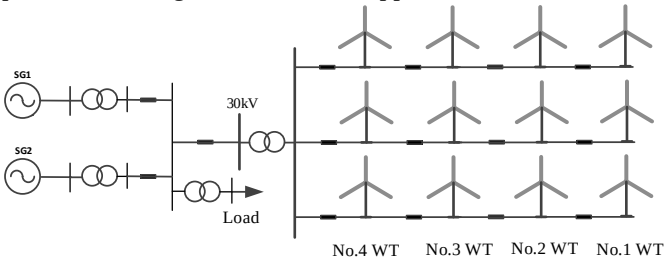

Fig. 6. Single-line diagram of test system

To investigate the effectiveness of the proposed adaptive power dispatch strategy, different wind speed conditions (i.e. low constant wind speed, high constant wind speed and variable wind speed) have been considered. Detailed results for three cases will be discussed in the following.

A. Case 1: Low Wind Speed Condition

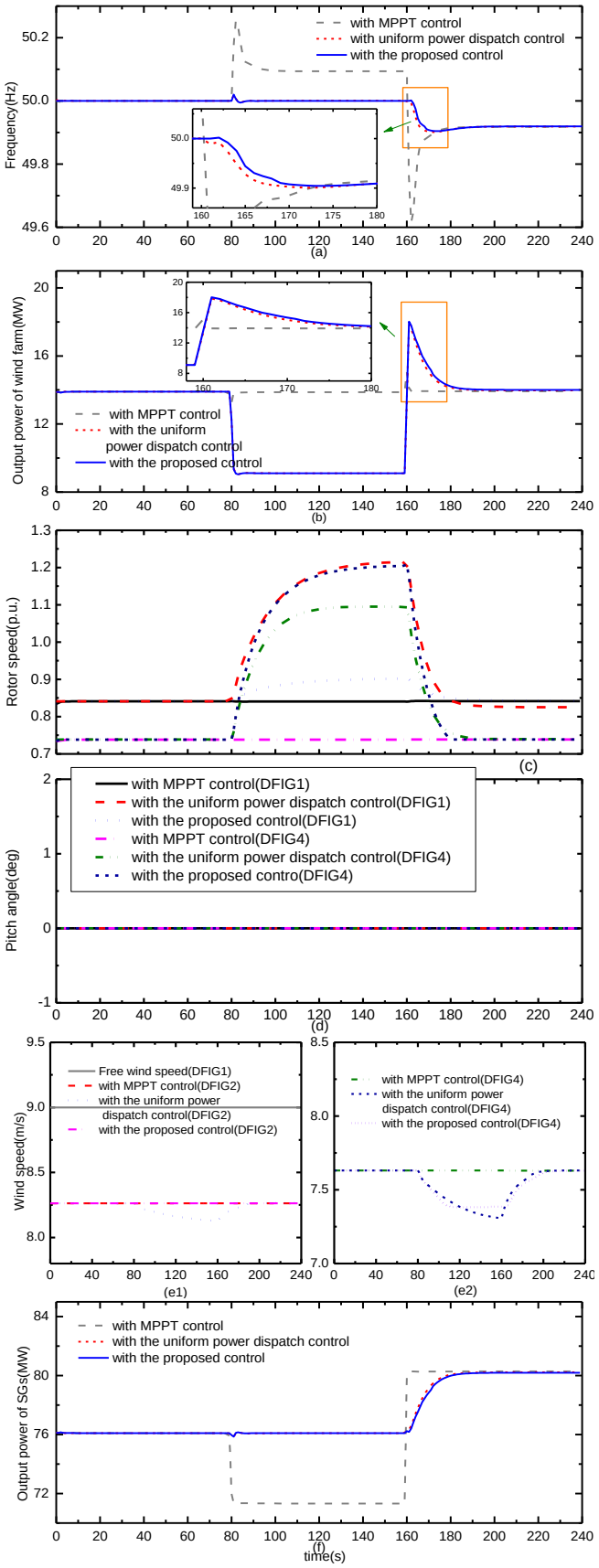

Fig. 7. Simulation results for case study with low constant wind speed. (a) System frequency, (b) WF output power, (c) DFIG rotor speed, (d) DFIG pitch angle, (e) Wind speed, (f) SGs output power

The concerned free wind speed is v_{w1}=9m/s. The load demand is set as 90-MW initially, a sudden load decrease (4.8-MW) event occurs in the testing system at t=80s and a sudden load increase(9-MW) event occurs at t=160s. We compare the uniform power dispatch method (i.e. the regulation task is sent to each WT equally) and our proposed method through simulation. Fig. 7 shows the results for case 1. It can be observed that the frequency behaviour is the worst with the MPPT control (frequency peak is 50.253Hz and the quasi-steady state frequency is 50.094Hz), as the WF does not provide any active power regulation service for system. In load sudden decrease event, the WF generation decreases with both the uniform power dispatch strategy and the proposed strategy. As a result, system frequency maintains at 50Hz throughout the load increase event. As the total KE charging range of WTs is large enough and the required deloading can be achieved via the overspeed control, the pitch angle control does not need to activate in both uniform deloading control and the adaptive deloading control. However, different from the uniform deloading strategy, the proposed strategy has a high utilization priority for downstream WTs' over-speed control. Hence it can be seen from Fig. 7(c) that the rotor speed of down-WTs accelerates to a higher value than up-WTs. As a result, the total KE storage in the WF is larger with the proposed deloading control than with the uniform deloading control according to the wake characteristic illustrated in Section IV. The WF can provide more active power support in turn when required. In load sudden increase event, it can be observed that the frequency nadir increases from 49.616Hz to 49.905Hz with the proposed control strategy, while the improvement is 284mHz with the uniform dispatch strategy. The rotor speed of each WT is decelerated to the value under MPPT mode as Fig. 7(c) indicated. The SGs' output power curve is shown in Fig. 7(f), it can be found that after WF participating in system active power regulation, their mechanical power can remain unchanged when load decrease event happens. While in load increase event, the mechanical power from the governor increases slower with the proposed control than that with the uniform power dispatch control. The influence of wake interactions on effective wind speed reaching down WTs can be seen in Fig. 7(e).

B. Case 2: High Wind Speed Condition

In this case, a 12m/s free wind speed is considered. The load variation events are the same with case 1. It can be observed that the power mismatch between load and generation is completely compensated in both the uniform and adaptive deloading control and system frequency maintains at 50Hz throughout the load increase disturbance. However, in the uniform power dispatch control scheme, the pitch angle control of DFIG 1 is activated to achieve the equally distributed deloading, which is due to its relatively high initial rotor speed. In contrast, when the proposed control is introduced, the KE based deloading capability of back-row WTs is fully utilized as the deloading task is allocated adaptively according to the KE charging range of each WT. Hence the pitch angle of front-row WTs does not need to activate. The load increases by 9-MW at *t*=160s. It is clearly seen from Fig. 8(a) that the system

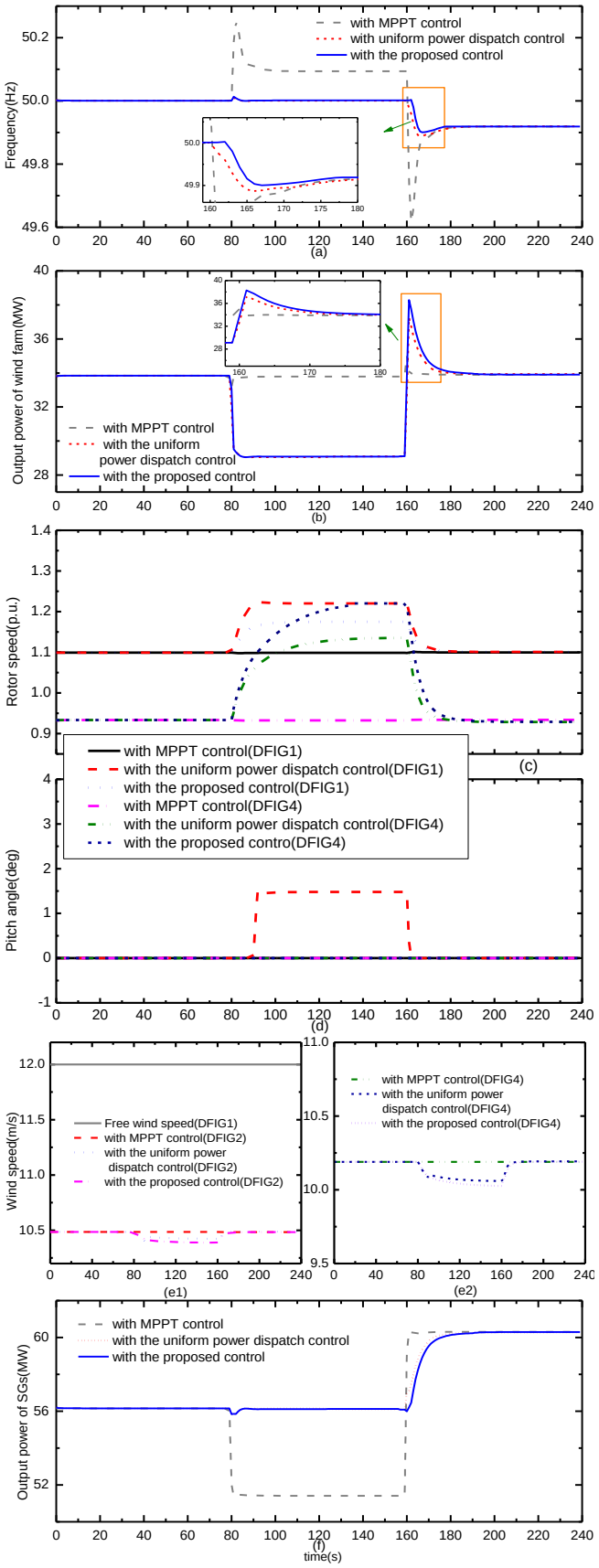

Fig. 8. Simulation results for case study with high constant wind speed. (a) System frequency, (b) WF output power, (c) DFIG rotor speed, (d) DFIG pitch angle, (e) Wind speed, (f) SGs output power

frequency deviation is the smallest and recovers fastest with the proposed control. By comparison, the frequency nadir increases to 49.9Hz with the proposed control, while frequency nadir is 46.887Hz with the uniform power dispatch control. This is because more KE is stored with the proposed control, and then more active power support can be provided in load increase event, as shown in Fig. 8(b).

C. Performance During Variable Wind Speed Condition

A set of fluctuated wind speed data for 300s is shown in Fig. 8(e) to assess the active power regulation contribution provided by WF. We evaluate the active power regulation performance of different control strategies by comparing the following four aspects: *total energy harvesting, total amount of pitch regulation, total amount of pitch angle actuation time, standard frequency deviation and standard dispatch command deviation (i.e. the standard dispatch command deviation is quantified to evaluate the active power regulation performance, which is defined as:* $\delta = \sqrt{1/N\sum_{i=1}^{N}(P_{\mathrm{WF}}^{act} - P_{WF}^{com})^2}$ *,where N is the total sampling amount, which is 300 in this case)* . Simulation results are summarized in Tables I and shown in Figs. 9.

TABLE I Comparisons of Simulation Results

	MPPT control	Uniform power dispatch	The proposed control
Total captured wind energy(kwh)	1713.52	1629.85	1639.02
Total amount of pitch regulation(deg)	250.59	588.51	401.64
Total amount of pitch angle actuation time(s)	123	324	174
Standard frequency deviation (Hz)	0.23	0.11	0.09
Standard dispatch command deviation	4.84	2.76	2.51

As reported in table I, the total wind energy harvesting with the proposed control strategy is larger than the simulation result with the uniform power dispatch method. It effectively validates that the proposed control is more energy-efficient. This is because the KE storage capability is adequately exploited in deloading situations via the proposed adaptive power regulation task allocation method. Subsequently, more additional active power can be provided in overloading situations, which can be seen Fig. 9(a). Since the KE based rotor speed control always has a high priority to utilize, the total amount of pitch regulation and total amount of pitch angle actuation time with the proposed control are reduced significantly compared with the uniform power dispatch method. It is easy to conclude that the mechanical fatigue of WTs is remarkably lower down while fulfill the dispatch command. To show the dynamic operation status of each WT during active power regulation process, behaviors of the rotor speed and pitch angle are shown in Fig. 9(c) and (d). It is clearly seen that rotor speed of back row WTs is lower and pitch angle of front WTs activates more frequently with the uniform power dispatch method as the KE of down-WTs is always not fully charged. When overloading is needed, the stored KE is released back to system via rotor speed deceleration. As shown in Fig.

9(c), the excessive rotor speed deceleration is avoided and hence the stable operation of WTs is guaranteed due to Eqs. (27-29). Compared with the MPPT control, system frequency fluctuations are effectively mitigated through the uniform power dispatch method and the proposed control. By comparison, it can be said that the proposed control has a better frequency regulation effect as Fig. 9(1) and Table I indicated. Since system frequency becomes smoother after wind farm participating in active power regulation, the frequency regulation burden of SGs is reduced and their power output fluctuations are diminished significantly, which can be seen in Fig. 9(f). As a result, their tear and wear and the operation and maintenance costs can be lower down. The impact of up-WTs' operation on wind speed reaching down-WTs is illustrated in Fig. 9(e). According to simulation results, it can be concluded that the active power regulation task of each WT can be adaptively allocated with the proposed control. Besides, the total wind energy loss and mechanical stress of WTs are reduced while provide active power regulation service.

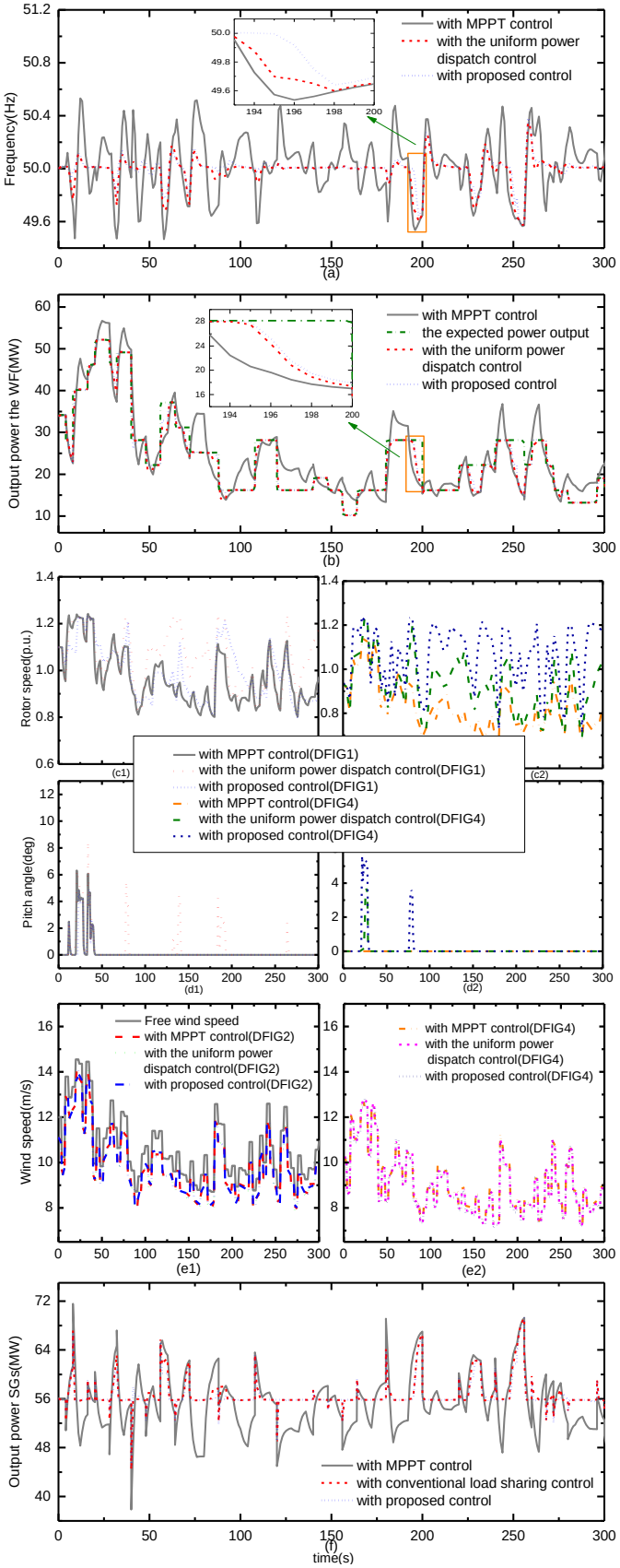

Fig. 9. Simulation results for case study with time-varying wind speed. (a) System frequency, (b) WF output power, (c) DFIG rotor speed, (d) DFIG pitch angle, (e) Wind speed, (f) SGs output power

VI. Conclusion

This paper proposes a novel control strategy to enable the WF to comply with the dispatch order, which inherently takes wake effect into account. Considering WTs operation status varies within the WF due to wake effect, an adaptive method to allocate the active power regulation task to individual WTs is proposed. Firstly, the deloading/overloading task allocation priority for each row WTs is determined according to the wake interaction characteristic. In addition, a KE storage estimation module is set up to adequately exploit the variable rotor speed range as an energy buffer in deloading situation and to guarantee WTs stable operation in overloading situation. The proposed control strategy is tested in a WF and simulation results show its promising performance in enhancing total energy harvesting and alleviating frequent pitch action while providing active power regulation ancillary service.

VII. Appendix

TABLE II Parameters of DFIG-based Wind Turbine

Symbol	Item	Value
T_β	Time constant of the pitch serve	0.5 s
H	Inertia constant	4s
P_{rated}	Rated power	5 MW
U_q	Terminal Voltage	3.3 kV
C	Capacitance of DC-link capacitor	4813μF
$U_{dcrated}$	Rated DC-link voltage	1.15kV
ω_{rmin}	Lower limit of rotor speed	0.7p.u.
ω_{rmax}	Upper limit of rotor speed	1.22p.u

TABLE III Parameters of SGs

Symbol	Item	Value
S_{g1}	Rated MVA	90MVA
S_{g2}	Rated MVA	30MVA
U_q	Terminal Voltage	30 kV
H_{g1}	Inertia Time constant	8.7s
H_{g2}	Inertia Time constant	4s
R_P	Turbine permanent droop	0.04
T_r	Governor time constant	8.408s
T_{servo}	Servo-motor time constant	0.5s
K_{gain}	Exciter regulator gain	400
T_e	Exciter time constant	0.01s

VIII. References

[1] K. Moslehi and R. Kumar, "A reliability perspective of the smart grid," *IEEE Transactions on Smart Grid*, vol. 1, no. 1, pp. 57-64, 2010.

[2] C. Jauch, A. Gloe, S. Hippel, and H. Thiesen, "Increased Wind Energy Yield and Grid Utilisation with Continuous Feed-In Management," *Energies*, vol. 10, no. 7, p. 870, 2017.

[3] M. Tsili and S. Papathanassiou, "A review of grid code technical requirements for wind farms," *IET Renewable power generation*, vol. 3, no. 3, p. 308, 2009.

[4] M. A. Abdullah, K. M. Muttaqi, D. Sutanto, and A. P. Agalgaonkar, "An effective power dispatch control strategy to improve generation schedulability and supply reliability of a wind farm using a battery energy storage system," *IEEE Transactions on Sustainable Energy*, vol. 6, no. 3, pp. 1093-1102, 2015.

[5] T. Caldognetto, P. Tenti, A. Costabeber, and P. Mattavelli, "Improving microgrid performance by cooperative control of distributed energy sources," *IEEE Transactions on Industry Applications*, vol. 50, no. 6, pp. 3921-3930, 2014.

[6] Q. Cao, Y.-D. Song, J. M. Guerrero, and S. Tian, "Coordinated control for flywheel energy storage matrix systems for wind farm based on charging/discharging ratio consensus algorithms," *IEEE Transactions on Smart Grid*, vol. 7, no. 3, pp. 1259-1267, 2016.

[7] Y. Xia, Y. Peng, P. Yang, M. Yu, and W. Wei, "Distributed Coordination Control for Multiple Bidirectional Power Converters in a Hybrid AC/DC Microgrid," *IEEE Transactions on Power Electronics*, vol. 32, no. 6, pp. 4949-4959, 2017.

[8] G. Diaz, P. G. Casielles, and C. Viescas, "Proposal for optimising the provision of inertial response reserve of variable-speed wind generators," *IET Renewable Power Generation*, vol. 7, no. 3, pp. 225-234, 2013.

[9] D. Ochoa and S. Martinez, "Fast-Frequency Response provided by DFIG-Wind Turbines and its impact on the grid," *IEEE Transactions on Power Systems*, vol. 32, no. 5, pp. 4002-4011, 2017.

[10] S. Wang, J. Hu, X. Yuan, and L. Sun, "On inertial dynamics of virtual-synchronous-controlled DFIG-based wind turbines," *IEEE Transactions on Energy Conversion*, vol. 30, no. 4, pp. 1691-1702, 2015.

[11] H. Ye, W. Pei, and Z. Qi, "Analytical modeling of inertial and droop responses from a wind farm for short-term frequency regulation in power systems," *IEEE Transactions on Power Systems*, vol. 31, no. 5, pp. 3414-3423, 2016.

[12] R. M. Kamel, A. Chaouachi, and K. Nagasaka, "Three control strategies to improve the microgrid transient dynamic response during isolated mode: A comparative study," *IEEE Transactions on Industrial Electronics*, vol. 60, no. 4, pp. 1314-1322, 2013.

[13] P. Moutis, S. A. Papathanassiou, and N. D. Hatziargyriou, "Improved load-frequency control contribution of variable speed variable pitch wind generators," *Renewable Energy*, vol. 48, pp. 514-523, 2012.

[14] E. Valsera‐Naranjo, A. Sumper, O. Gomis‐Bellmunt, A. Junyent‐Ferré, and M. Martínez‐Rojas, "Pitch control system design to improve frequency response capability of fixed‐speed wind turbine systems," *International Transactions on Electrical Energy Systems*, vol. 21, no. 7, pp. 1984-2006, 2011.

[15] C. Jauch and S. Hippel, "Hydraulic–pneumatic flywheel system in a wind turbine rotor for inertia control," *IET Renewable Power Generation*, vol. 10, no. 1, pp. 33-41, 2016.

[16] W. Zhang, Y. Xu, W. Liu, F. Ferrese, and L. Liu, "Fully distributed coordination of multiple DFIGs in a microgrid for load sharing," *IEEE Transactions on Smart Grid*, vol. 4, no. 2, pp. 806-815, 2013.

[17] P. Kou, D. Liang, and L. Gao, "Distributed Coordination of Multiple PMSGs in an Islanded DC Microgrid for Load Sharing," *IEEE Transactions on Energy Conversion*, vol. 32, no. 2, pp. 471-485, 2017.

[18] H. Wang, Z. Chen, and Q. Jiang, "Optimal control method for wind farm to support temporary primary frequency control with minimised wind energy cost," *IET Renewable Power Generation*, vol. 9, no. 4, pp. 350-359, 2014.

[19] Y. Li, Z. Xu, J. Zhang, H. Yang, and K. P. Wong, "Variable Utilization Level Scheme for Load Sharing Control of Wind Farm," *IEEE Transactions on Energy Conversion*, 2017.

[20] X. Gao, K. Meng, Z. Y. Dong, D. Wang, M. El Moursi, and K. Wong, "Cooperation-Driven Distributed Control Scheme for Large-scale Wind Farm Active Power Regulation," *IEEE Transactions on Energy Conversion*, 2017.

[21] R. G. De Almeida, E. D. Castronuovo, and J. P. Lopes, "Optimum generation control in wind parks when carrying out system operator requests," *IEEE transactions on power systems*, vol. 21, no. 2, pp. 718-725, 2006.

[22] F. González-Longatt, P. Wall, and V. Terzija, "Wake effect in wind farm performance: Steady-state and dynamic behavior," *Renewable Energy*, vol. 39, no. 1, pp. 329-338, 2012.

[23] J. Jonkman, S. Butterfield, W. Musial, and G. Scott, "Definition of a 5-MW reference wind turbine for offshore system development," *National Renewable Energy Laboratory, Golden, CO, Technical Report No. NREL/TP-500-38060*, 2009.

[24] T. Ackermann, *Wind power in power systems*. John Wiley & Sons, 2005.

[25] N. A. Janssens, G. Lambin, and N. Bragard, "Active power control strategies of DFIG wind turbines," in *Power Tech, 2007 IEEE Lausanne*, 2007, pp. 516-521: IEEE.

Lyu Xue (S'16) received her B.Eng. degree from Qingdao University of Technology, China, in 2013; and M. Eng. degree from Shanghai University of Electric Power, China, in 2016. She is currently working toward the Ph.D. degree in the Department of Electrical Engineering, The Hong Kong Polytechnic University, Hong Kong. She is also a visiting PhD student in the Department of Electrical and Electronic Engineering, Southern University of Science and Technology, Shenzhen, China. Her research interests include advanced modeling and control for grid-integration of renewable energy systems and energy internet.

Youwei Jia (S'11, M'15) received his B.Eng and Ph.D degrees from Sichuan University, China, in 2011, and The Hong Kong Polytechnic University, Hong Kong, in 2015, respectively. From 2015 to 2018, he was a postdoctoral fellow at The Hong Kong Polytechnic University. He is currently an Assistant Professor with the Department of Electrical and Electronic Engineering, Southern University of Science and Technology, Shenzhen, China. His research interests include microgrid, renewable energy modeling and control, power system security analysis, complex network and artificial intelligence in power engineering.

Zhao Xu (M'06-SM'12) received B.Eng, M.Eng and Ph.D degree from Zhejiang University, National University of Singapore, and The University of Queensland in 1996, 2002 and 2006, respectively. From 2006 to 2009, he was an Assistant and later Associate Professor with the Centre for Electric Technology, Technical University of Denmark, Lyngby, Denmark. Since 2010, he has been with The Hong Kong Polytechnic University, where he is currently a Professor in the Department of Electrical Engineering and Leader of Smart Grid Research Area (http://www.mypolyuweb.hk/eezhaoxu/). He is also a foreign Associate Staff of Centre for Electric Technology, Technical University of Denmark. His research interests include demand side, grid integration of wind and solar power, electricity market planning and management, and AI applications. He is an Editor of the Electric Power Components and Systems, the IEEE PES Power Engineering Letter, and the IEEE Transactions on Smart Grid. He is currently the Chairman of IEEE PES/IES/PELS/IAS Joint Chapter in Hong Kong Section.